

SEA SURFACE SIMULATOR FOR TESTING A SYNTHETIC APERTURE SONAR

B. DAVIS

University of Arizona, Tucson, AZ

P. GOUGH

University of Canterbury, Christchurch, New Zealand

E-mail: gough@elec.canterbury.ac.nz

B. HUNT

University of Arizona, Tucson, AZ

With the move to use side-looking imaging sonars in very shallow waters as a component part of MCM operations, synthetic aperture sonars (SAS) appear to have some advantages over a conventional real aperture side-looking sonars. One significant advantage of SAS is that it is quite resilient to image degradation caused by surface backscatter and surface multipath. The processing in all SAS imaging algorithm assumes the only thing moving between transmitted pings is the sonar platform. Since the algorithm uses coherent integration to assemble the final image, any movement of the sea surface between pings destroys the ping-to-ping coherence of the surface multipath as well as the ping-to-ping surface backscattered return. To move towards understanding just how effective a SAS is at suppressing backscatter and surface multipath, we first need to model the moving sea surface in a believable way and establish just how the sound reflects off the undersurface of the sea. This paper first describes a commonly-used physically justifiable sea-surface autocorrelation function that accounts for wind direction, wave height, wave period and wave velocity. From this autocorrelation function, a statistically appropriate random wave surface is generated which evolves in both time and space. Finally in a first attempt to model the shallow-water sea surface multipath problem, a set of impulse responses are generated from this wave-surface as it evolves in time increments equal to the pulse repetition period. Here we model an isotropic one-way (reflected) acoustic path from the target at a depth of seven metres to the sonar platform at a depth of five metres separated by 25m with the surface above the path covering an area of 160m (cross-track) by 60m (along-track) and we ignore any seafloor multipath. Two sea-surface reflection/scattering mechanisms are used in this model. In the first, each surface facet acts as a diffraction-limited aperture and in the second, each facet acts as a Lambertian reflector. These describe two limiting situations 1) when the acoustic wavelength is small compared with the roughness of any facet and 2) when the surface roughness is a significant proportion of the acoustic wavelength. Concentrating on the diffraction-limited model, we show the effect of surface multipath on the raw data collected by a SAS and its effect on the processed image. We also make some estimates of the signal to clutter ratio improvements as a function of the number of hits on target.

1 Introduction

The imaging fidelity of any standard side-looking sonar is degraded by sea surface backscatter and sea-surface multipath reflections as well as seafloor multipath reflections as shown in Figure 1, however, surface backscatter and multipath are different in that they change with time. By using synthetic aperture sonar (SAS) techniques, we can use the time-variable nature of the sea surface to our advantage.

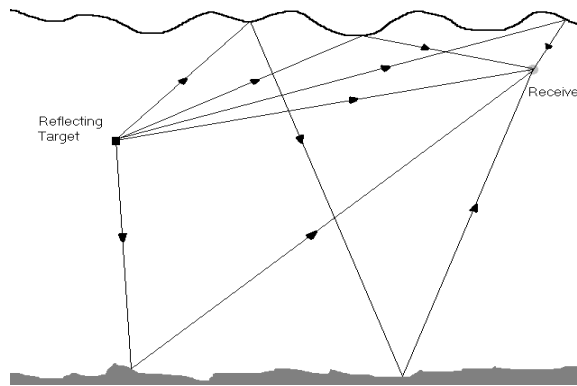


Figure 1. Illustrating sea surface and seafloor multi-path reflections

All SAS systems record the pulse echo returns from each transmitted ping in both amplitude and phase so they can, by using coherent integration, compute an image from a contiguous collection of ping echoes as if it came from a much larger physical aperture. For SAS to work there are some critical assumptions. The first is that the platform moves in a predictable and usually linear track. A combination of highly accurate navigation units and autofocus techniques (sometimes called micro navigation) can now correct the problems caused by nonlinear track. The second assumption, and the one pertinent to this paper, is that the only thing moving during the collection of the data is the sonar platform. Since the sea-surface is clearly moving, it is important to establish how this movement affects the data collected and more importantly how it effects the final image. To do this, we normally simulate the complete sonar data collection and imaging system both with and without the sea-surface effects but to do this we need to model the sea-surface in a believable way. Unfortunately if all the multipath effects are included in the simulation, the model becomes extremely complicated so we restrict our simulations to consider only the effects of sea-surface multipath on the reflected echoes. That is we assume the vertical beamwidth of the projector is small enough to eliminate any surface backscatter and sea-surface multipath on the outward leg of the acoustic path and that there are no sea-floor multipath effects. Despite these limitations, we believe the simulations show realistic effects of sea-surface multipath and how it effects the SAS imaging process.

2 The autocorrelation of the sea surface

A useful model of the space and time autocorrelation of the sea surface already exists and we use it here without proof [1]

$$R_S(\zeta, \eta, \tau) = A_D^2 \exp\left[-\frac{(\zeta - u_G\tau)^2}{L_w^2}\right] \exp\left[-\left(\frac{\eta}{L_c}\right)^2\right] \cos[K_w\zeta - \Omega\tau] \quad (1)$$

with related variables -

w	windward direction
c	cross wind direction
ζ	windward ordinate in m
η	crosswind ordinate in m
τ	temporal delay ordinate in s
A_D	<i>RMS</i> displacement amplitude in m
L_w	windward correlation length in m
L_c	crosswind correlation length in m
L_t	temporal correlation time in s
K_w	spatial frequency in windward direction in m^{-1}
Ω	temporal frequency in s^{-1}
$u_G = \frac{L_x}{L_t}$	group velocity of waves in ms^{-1}
$u_P = \frac{\Omega}{K_w}$	phase velocity of waves in ms^{-1} .

Basically the wave crests are assumed to be correlated in the windward and crosswind direction and move with an average velocity in the windward direction. Here w,c represent the windward and crosswind coordinates which will eventually be rotated into the imaging coordinates of x and y . In addition, measurements show that the distribution of displacements at a given point is approximately Gaussian [1] and stationarity is also assumed. A single example of a sea surface is shown in fig.2 with the following parameters: crosswind correlation length 12m, windward correlation length 7m, dominant windward wavenumber 2m^{-1} , temporal frequency 2Hz, RMS wave amplitude 0.2m and wind direction 126° to the x axis.

3 Tiling the surface

The simulated sea surface needs to be tiled into a contiguous set of reflecting facets. The easiest way to do this is to tile the surface into triangular surface elements; the three vertices of the triangle being defined by three x, y, z coordinates. The three vertices then define a tilted triangular facet. This can be specified to any aspect ratio down to the smallest facet delimited by the rectangular sampling grid with separation Δx and Δy .

Having constructed a single realisation of the sea-surface, $s(w, c, t)$, and having determined the distance (and so delay time) from the transmitter to the target and from the target to the surface facet at x_0, y_0 then from the surface to the receiver as well as the vector-dependent facet gain term, $G_L(x_0, y_0)$ (for Lambertian scattering) or $G_D(x_0, y_0)$ for diffraction-limited scattering), it remains to add the contributions from all the surface facets to calculate the impulse response of the sea surface.

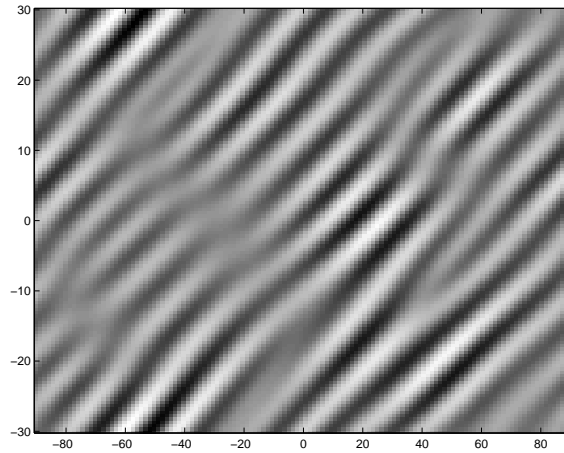


Figure 2. Example of a typical simulated sea surface

4 Simulation Results

Before we simulate the effects of time-varying multipath on SAS imaging, it is useful to visualise the modulus of the facet gain term $|G_D|$ and $|G_L|$ as a function of x_0, y_0 as well as its impulse response for a specific surface condition. A useful limiting case to check is that of a “fat” sea-surface. Clearly for Lambertian scattering to exist at all, there would be some capillary waves present to drive the scattering mechanism. Since there are far too many parameters to perturb, we chose to model a specific situation with a target at a depth of 10m with a receiver at a depth of 10m, the two separated by 100m using a centre transmitted frequency of 100kHz. As expected, the Lambertian model showed little or no variation with facet size and carrier frequency whereas the diffraction-limited model showed a change in the sinc pattern as would be expected by changing the ratio of wavelength to aperture size.

When the surface has some non-zero wave height, some interesting behaviour is revealed. Figure 3 shows the gain-modulus image for a sea surface with a Lambertian scattering model. This image has the same general trend as the “fat” surface case but with the wave structure imposing lengths of minimal or zero gain. These structures tend to be more dense away from the area directly between the target and receiver.

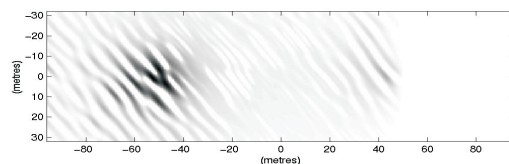


Figure 3. Gain-modulus image for a sea surface with Lambertian scattering

The gain-modulus image for a sea surface using the diffraction-limited model is shown

SEA SURFACE SIMULATION

in fig.4. It resembles its flat surface counterpart but does have significant effects present attributable to the wave structure. Like the Lambertian case, the tilts of the facets have the effect of reducing the gain in certain places.

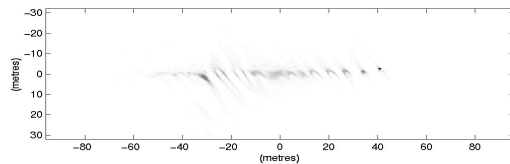


Figure 4. Gain-modulus image for a sea surface with diffraction-limited scattering

5 Modelling a SAS

First we make the assumption that there is no movement during the transmission and reception of a single pulse and that all movements of the surface and the sonar are condensed into a single instantaneous period between the last echo return of one ping and the onset of transmission of the next ping. This is known as the “stop and hop” scenario. This does ignore any temporal Doppler effects that occur due to movement during a pulse. Since existing SAS seldom operate at maximum unambiguous ranges of more than 200m, they mostly use a pulse repetition period of shorter than 300 ms consequently we consider “stop and hop” scenario accurate enough to model surface multipath effects.

To model the surface effects on the imaging process, we proceed in the following fashion. A point target layout is selected which represents a typical target location and depth along with the SAS parameters and the surface conditions needed to compute the sea surface autocorrelation function. The surface realisation $s(w, c, t)$ is computed and we record the impulse response for the particular position of the sonar relative to the target(s). Then the sonar is moved by Δu and the surface evolved in time by $\Delta T = \Delta u/v_s$ where v_s is the forward velocity of the sonar platform. This process is repeated for every ping as the sonar traverses a single pass of the target field. It is also repeated over a range of differing surface conditions using both Lambertian and diffraction limited scattering.

Using a simulated target field of three point-reflectors gives a basis for comparison and fig.5 shows the intensity of raw data echo returns displayed in dB intensity to bring out the features normally concealed in a linear display. Now a surface multipath using the diffraction model is factored into the data and is shown in fig.6. Note the waveheight in the sea surface, 1m, is enough to show the existence of the multipath but not so much as to overwhelm the underlying raw data. Also note that the multipath appears to have produced some “structured” echoes that could easily be misinterpreted. This is most easily seen in that there appears to be a fourth target to the right of the central target. In addition the multipath of the upper target overlays the central target and if the multipath were stronger, would conceal it.

To get some estimate of the all-important signal-to-clutter ratio (SCR), we can take an ensemble line scan in range (i.e that is along the fast-time or cross-track axis) through

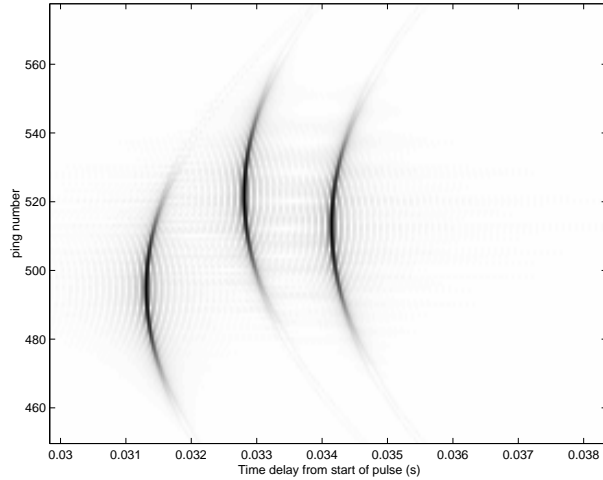


Figure 5. Image intensity of raw data (dB scale) for 3 point reflectors with no multipath

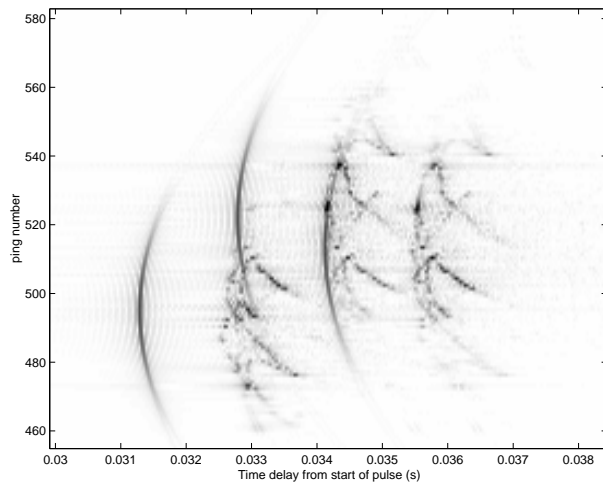


Figure 6. Image intensity of the same raw data corrupted by surface multipath

the centre of the target echo shown in fig.6. The SCR can be estimated from the RMS value of the target's direct path return followed by the RMS surface multipath return. By looking closely at the clutter surrounding the central unprocessed return, we estimate the SCR caused solely by multipath (since there is no other clutter mechanism) to be about 10dB.

Now the raw data is processed to a final image intensity and displayed in fig.8. Note there are about $p=40$ pings on target so if we were to expect all the target returns to add coherently i.e., a $20 \log(p)$ increase in peak intensity, and all the multipath clutter to add non-coherently by $20 \log(p^{0.5})$, we would expect a 16dB improvement in SCR. So by taking the RMS value of the pixels surrounding the central target in the processed image, we estimate the SCR to be about 20dB ; a 10db improvement over the 10dB SCR of the

SEA SURFACE SIMULATION

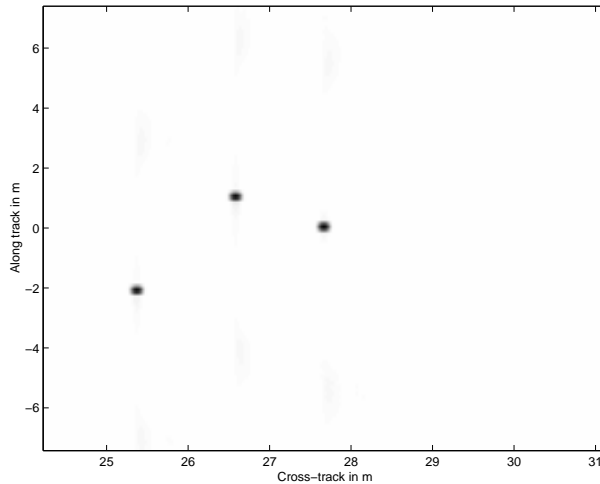


Figure 7. Image intensity of azimuth compressed data (dB scale) for 3 point reflectors with no multipath

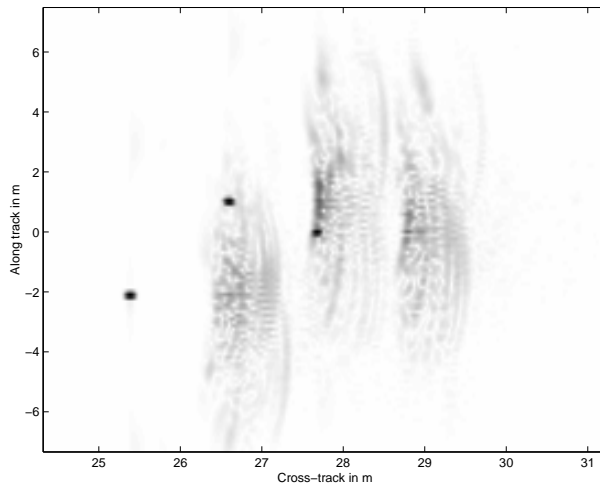


Figure 8. Image intensity of same azimuth compressed data corrupted by surface multipath

raw data. In this way we can get a quantitative estimate of the improvement over the raw data image as a function of hits on target. Stated briefly

$$\text{SCR improvement} \approx 10 \log(p^{0.65}). \quad (2)$$

which indicates the surface multipath has some correlation from ping-to-ping.

6 Conclusions

In shallow waters, clutter caused by surface multipath limits the image quality of all side-looking sonars. However, SAS have a significant advantage in the the echo returns from

many pings are processed coherently which means that there will be some improvement in the SCR in the processed image. The actual degree of improvement in SCR ratio is dependent on how fast the surface changes with respect to the pulse repetition period but, for our hypothetical surface, target layout and sonar parameters, the improvement appears to be about $10 \log(p^{0.65})$.

References

1. H. Medwin and C.S. Clay, *Fundamentals of Acoustical Oceanography*, Applications of Modern Acoustics. Academic Press, San Diego, California, 1998.
2. J.C. Novarini and J.W. Caruthers, Numerical modeling of acoustic-wave scattering from randomly rough surfaces: An image model, *The Journal of the Acoustical Society of America*, vol. 53, no. 3, pp. 876–884, 1973.
3. J.C. Novarini and H. Medwin, Diffraction, reflection, and interference during near-grazing and near-normal ocean surface backscattering, *The Journal of the Acoustical Society of America*, vol. 64, no. 1, pp. 260–268, July 1978.
4. W.A. Kinney, C.S. Clay, and G.A. Sandness, Scattering from a corrugated surface: Comparison between experiment, Helmholtz-Kirchoff theory, and the facet-ensemble method, *The Journal of the Acoustical Society of America*, vol. 73, no. 1, pp. 183–194, January 1983.
5. D.W. Hawkins and P.T. Gough, Recent sea trials of a synthetic aperture sonar, *Proceedings of the Institute of Acoustics*, vol. 17, no. 8, pp. 1–10, December 1995.
6. D.W. Hawkins, *Synthetic Aperture Imaging Algorithms: With Application to Wide Bandwidth Sonar*, Ph.D. thesis, Electrical and Electronic Engineering, University of Canterbury, Christchurch, New Zealand, October 1996.
7. P.T. Gough and D.W. Hawkins, Unified framework for modern synthetic aperture imaging algorithms, *The International Journal of Imaging Systems and Technology*, vol. 8, pp. 343–358, 1997.
8. Mehrdad Soumekh, *Fourier Array Imaging*, Prentice Hall, Englewood Cliffs, New Jersey, 1994.
9. J.R. Schott, *Remote Sensing: The Image Chain Approach*, Oxford University Press Inc., New York, New York, 1997.
10. J.W. Goodman, *Introduction to Fourier Optics*, Electrical and Computer Engineering: Electromagnetics. McGraw Hill, New York, New York, 2nd edition, 1968.
11. P. Beckmann and A. Spizzichino, *The Scattering of Electromagnetic Waves from Rough Surfaces*, Macmillan, New York, New York, 1963.